Research Article Vol. 3, No. 7 / July 2016 / Optica 787

Luminescent detector for free-space optical communication

T. Peyronel, K. J. Quirk, S. C. Wang, and T. G. Tiecke*

Facebook Inc., Connectivity Lab, 1 Hacker Way, Menlo Park, California 94025, USA
**Corresponding author: ttiecke@fb.com*

Received 21 March 2016; revised 25 May 2016; accepted 26 May 2016 (Doc. ID 261445); published 19 July 2016

Free-space optical communication holds the promise of high-throughput wireless communication channels for long distances as well as for short-range indoor applications. To fully benefit from the high data rates enabled by optical carriers, the light needs to be efficiently collected onto a fast photodetector, which requires complex pointing and tracking systems. Here, we show that fluorescent materials can be used to increase the active area of a photodiode by orders of magnitude while maintaining its short response time and increasing its field of view. Using commercially available materials, we demonstrate a detector with an active area of 126 cm^2 achieving data rates up to 2.1 Gbps at an eye-safe intensity. We demonstrate a detector geometry with omnidirectional sensitivity and discuss the need for new materials tailored for communication applications.

OCIS codes: (060.2605) Free-space optical communication; (160.2540) Fluorescent and luminescent materials; (040.5160) Photodetectors; (060.4510) Optical communications.

http://dx.doi.org/10.1364/OPTICA.3.000787

1. INTRODUCTION

The need for high data rate wireless communication has rapidly increased over the past decade. While optical communications have become the *de facto* standard for high-throughput wired communication channels, microwave and millimeter wave carrier frequencies are still the standard for wireless links. However, the limited availability of spectrum restricts the data rates that can be achieved through these channels. To address this challenge, free-space optical communication has emerged as a promising method for both indoor and outdoor communication [1]. The use of optical carrier frequencies allows for many orders of magnitude more available spectrum, a high degree of spatial multiplexing [2,3], and the possibility to communicate at a high data rate in the absence of fiber network infrastructures, e.g., to space [4] or high-altitude unmanned aerial vehicles [5,6].

Semiconductor photodiodes are commonly used as optical detectors at high frequencies [7]. However, the response times of these diodes are limited by the junction capacitance and the carrier transit time, and scale with detector size. Achieving a bandwidth of the order of 1 GHz requires the use of detectors with an active area of at most ~1 mm^2, orders of magnitude smaller than the typical spatial extent of an optical mode after propagation through space. This mismatch can be compensated for by using focusing optics; however, the unequivocal trade-off is a reduced field of view because of the conservation of étendue in geometrical optics [8]. The loss of field of view associated with the necessary increased active aperture is usually compensated for by active pointing and tracking systems that add significant complexity and have arguably limited broader adoption of free-space optical communications. Alternative large active area photodetection technologies with fast response times include metal–semiconductor–metal (MSM) detectors and focal plane arrays. However, their restricted fabrication size and other limitations, such as limited availability or cost and complexity for light-sensing arrays, constrains their use in free-space optical systems.

Here, we present a method to increase the effective area and field of view of an optical receiver while maintaining fast response times. We achieve this by using optical waveguides doped with wavelength shifting dyes, also known as luminescent concentrators. The incident light, modulated with a communication signal, is absorbed by the dye molecules independently of the light incidence angle and subsequently re-emitted at a different wavelength. A portion of the emitted light is collected by the fiber and guided to a small area semiconductor photodiode. We refer to the combined system of the luminescent concentrators and photodiode as a *luminescent detector* (LD). The intermediate scattering by the molecular dye enables efficient collection of light over a large area and its concentration over an end facet with a reduced étendue. Étendue is a conserved quantity for geometrical optical systems and sets the maximum light concentration. However, in the presence of inelastic scattering, such as from a fluorescent dye, the étendue can be reduced, because the vibrational degrees of freedom of the dye molecule can carry away entropy during the inelastic scattering event [8]. This concept has been widely used to concentrate light for solar energy harvesting [9] and in detectors for high-energy physics experiments [10], but its potential has not yet been harvested for optical communications.

The use of luminescent concentrators can have a significant impact in this context: the detector has a large active area *and* a fast response time, allowing high-data-rate communication without the need for accurate pointing and tracking. Additionally, it has omnidirectional sensitivity and is insensitive to the spatial mode of the incident light, opening possibilities for mobile applications as well as using diffuse light sources or highly multimode optical fields (e.g., arising from propagation through a turbulent atmosphere). The emerging field of visible light communications [11] constitutes a particular area of interest. In this context, multi-Gbps communication links have been demonstrated using LEDs [12] in a static configuration using conventional photodiodes as detectors. One possible indoor application could be high-definition video streaming to mobile devices, which require high-data-rate channels and are intrinsically asymmetric links. As a possible outdoor application a long-range (kilometer length scale) point-to-point link using this detector concept could allow for relaxed sensitivity to atmospheric turbulence, building vibrations as well as low-cost deployment.

To demonstrate the potential of LDs, we perform a set of proof-of-concept experiments. We use commercially available scintillating fibers to build a large area (~100 cm^2), large field-of-view LD; we study its bandwidth properties and demonstrate a free-space optical communication system with a throughput of 2.1 Gbps under eye-safe illumination conditions. In addition, we use the same material to create a detector with omnidirectional sensitivity. Our results open new perspectives for free-space optical communications and call for the development of tailored luminescent materials that would allow >10 Gbps data rates.

2. RESULTS

Figures 1(a) and 1(b) show a typical LD: a tight array of polystyrene fibers doped with an organic dye (Saint-Gobain BCF-92) forms a rectangular detector with $w = 3.6$ cm and $L = 35$ cm, yielding an active area of $A_{LD} = 126$ cm^2. The wavelength shifting fiber has a square cross section of 0.5 mm × 0.5 mm. The concentration of dyes is chosen so that photons of wavelength ~405 nm impinging on the fibers are absorbed with near unity probability and re-emitted at ~490 nm [see Fig. 1(c)]. Some of the re-emitted photons are guided along the fibers through total internal reflection with negligible re-absorption due to the large Stokes shift, resulting in well-separated absorption and emission spectra. At the extremity, the fibers are bundled together to form a circular radiating surface of area $\pi \times 2.5^2$ mm^2 and a numerical aperture of NA = 0.54.

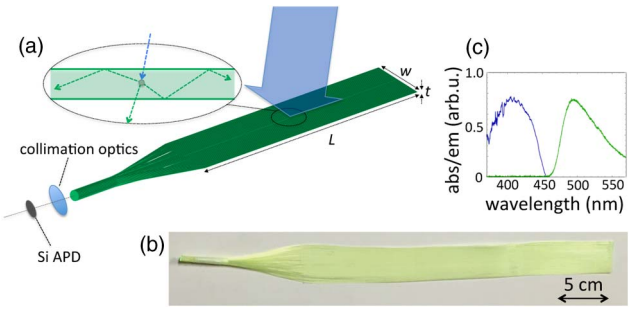

Fig. 1. (a) LD concept: the LD consists of plastic optical fibers of 0.5 mm × 0.5 mm cross section, aligned in a planar array of width w, length L and thickness t. The optical fibers are doped with an organic dye and illuminated with a large optical beam (blue arrow). The dye molecules absorb and re-emit the light partly into guided modes of the fibers (green arrows, inset), and the guided light is subsequently concentrated using optical elements onto a small-area APD. The optical signal is modulated to carry a communication signal, which is detected by the photodiode. (b) Photograph of the LD as used for the measurements in Figs. 2 and 3 (see text). (c) Absorption (blue) and emission (green) spectra of the organic dye. The spectra are well separated, leading to negligible re-absorption of the scattered light.

A. Figures of Merit

Typically, for communication applications, the collection efficiency, noise power, and bandwidth determine the achievable throughput and constitute the figures of merit for the detector [7].

1. Efficiency

First, we turn to the efficiency; assuming the light is emitted isotropically by the dye molecules, only a fraction of the solid angle is scattered at angles that are below the critical angle for total internal reflection. The capture efficiency η_c of the LD depends on the refractive index of the waveguide and cladding materials, as well as on the shape of the fiber. Our rectangular fiber has refractive indices of the cladding (core) of $n_{cl} = 1.49$ ($n_{co} = 1.60$), yielding a capture efficiency of $\eta_c = 4.5\%$ per direction. Additional losses arise from the quantum efficiency of the dye molecules and imperfect outcoupling of the fiber facets. We measure a total conversion efficiency $\eta_{cnv} = 1.5\%$, which accounts for all the material-related efficiencies, including η_c, between the incident light and the light emitted from the fiber facet. A set of condenser lenses collects the light exiting the fiber bundle with $\eta_{col} = 20\%$ efficiency (limited by the NA of the fiber) onto an avalanche photodiode (APD) with an active area of $A_{PD} = 3.1$ mm^2. Here, we use an APD, but the luminescent material can be used in conjunction with any type of photodetector, including MSM and focal plane array detectors. The light collection gain G_{LD} of the LD over the bare PD is given by the product of the active area gain and the overall efficiency:

$$G_{LD} = \frac{A_{LD}}{A_{PD}} \eta_{cnv} \eta_{col}. \quad (1)$$

For our specific detector, active area gain $A_{LD}/A_{PD} = 4.1 \times 10^3$ and efficiency of $\eta_{cnv}\eta_{col} = 0.3\%$ yield a light collection gain of $G_{LD} = 12.3$. The total efficiency can potentially exceed 10% with tailored materials and technical improvements, as will be discussed below. A similar active area gain with near-unity efficiency can be achieved with a conventional lens but comes at the expense of a reduced field of view.

2. Noise

Various effects contribute to the total noise on the received signal, including shot noise, Johnson noise, amplifier noise, nonlinearities, and, in the case of APDs, the excess noise factor, all contributing to the noise equivalent power (NEP) of the photodetector. Adding the luminescent material as an intermediate stage can potentially cause increased noise, which we address here. First, the reduced collection efficiency caused by the luminescent material increases the NEP of the LD with respect to the APD as $NEP_{LD} = NEP_{APD}/(\eta_{cnv}\eta_{col})$. Second, the luminescent dye fluorescence will saturate at high intensity, causing a nonlinear response. However, we measure a linear response of the dye up to 2.8 mW/cm^2, well above typical operating conditions; therefore, the luminescent material does not add nonlinearity to the

channel. Third, in this linear regime, the fluorescence follows Poisson statistics and therefore does not add excess noise to the photon shot noise. Finally, the increased étendue of the detector makes it collect more background light, which can limit its application in conditions where the noise floor is dominated by background light. Static and low-frequency variation of the background light can be easily rejected from a modulated communication signal; however, in applications with a large amount of background light and weak signals, the shot noise of the background light can become the dominant noise contribution. For the LD as shown in Fig. 1, we measure the noise spectral density (NSD) under normal indoor lighting conditions to be $\mathrm{NSD_{LD}} = -128.8$ dBm/Hz, equal to that of the APD itself in the absence of room light, $\mathrm{NSD_{APD}} = -129.2$ dBm/Hz [13], indicating that, for this design, background noise does not contribute to the noise floor. Also, we note that the absorption spectrum of the LD is less than 100 nm wide, and, therefore, only a fraction of the background light is detected.

3. Bandwidth

The bandwidth of the composite detector is determined by four processes. First, the rate of absorption and re-emission of the molecular dye is limited by the lifetime of the excited state, which follows an exponential decay process with time constant τ_e. Second, the travel time of the photons in the waveguide contributes to pulse spreading. For a uniform illumination of the fiber over a length L_i, the pulse broadening is uniform in time over the delay $\tau_s = L_i n_{\mathrm{co}}/c$, where c is the speed of light in vacuum. Third, additional pulse spreading arises from dispersion in the multimode fiber. For a small critical angle for total internal reflection and uniform illumination of the detector, this contribution is negligible compared to τ_s. The final contribution is the response of the photodiode and detection electronics, given by $H(\omega)$. The exponential decay processes lead to a Lorentzian frequency response, while uniform pulse spreading yields a sinc frequency response; hence, the total frequency response R_{LD} of the LD can be written as a product of the transfer functions of the individual processes:

$$R_{\mathrm{LD}}(\omega) = \frac{\mathrm{sinc}(\tau_s\omega/2)}{(1+\tau_e^2\omega^2)} H(\omega), \tag{2}$$

where $\omega = 2\pi \times f$ is the angular frequency. Note that the cut-off frequency, a normalized response of −3 dB, of a Lorentzian transfer function is at $f_{-3\,\mathrm{dB}} = 1/(2\pi\tau_e)$ and drops off slowly, while that of a sinc function is at $f_{-3\,\mathrm{dB}} \simeq 3.791/(2\pi\tau_s)$ with a much steeper drop at higher frequencies. A critical length scale $L_c \simeq 3.791\tau_e c/n_{\mathrm{co}}$ is defined as the length where the bandwidth of the LD is equally limited by its length, as well as the material bandwidth.

Figure 2(b) shows a measurement (see Supplement 1) of the step response of our material, yielding a fluorescence lifetime of $\tau_e = 1.77$ ns, corresponding to a 3 dB bandwidth of $f_{-3\,\mathrm{dB}} = 1/(2\pi \times 1.77\ \mathrm{ns}) = 91$ MHz. This yields $L_c = 1.26$ m; hence, only for very large detectors does the pulse spreading from the detector length become the dominant bandwidth limitation.

We measure the frequency response of the LD as a function of the area of the detector that is illuminated [see Fig. 2(a)]. For the largest illuminated length ($L = 254$ mm), the active area of the LD is 3 orders of magnitude greater than that of the bare photodiode without significantly sacrificing the bandwidth of the APD. The bandwidth of the LD is purely limited by the fluorescence lifetime of the material. Figure 2(c) shows the spectral response of the material, measured independently using a small (1 mm) illumination spot and a small, fast photodiode (see Supplement 1).

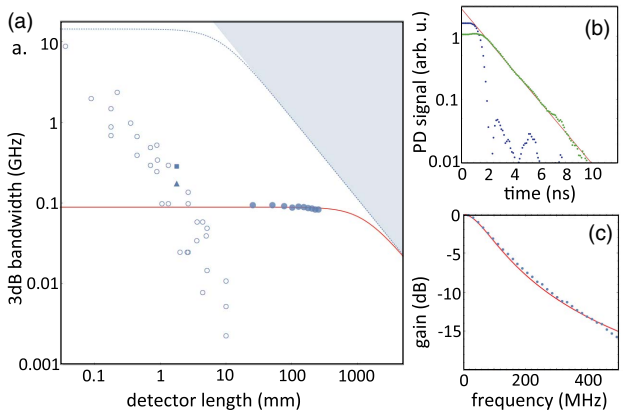

Fig. 2. (a) Bandwidth versus detector length. The blue solid circles are the measured 3 dB bandwidth for the detector in Fig. 1(b). The different points correspond to different illumination lengths. The solid square indicates the bare APD bandwidth [14] and the solid triangle the measured bandwidth of the detection electronics $H(\omega)$ (see Supplement 1). The red solid (respectively, blue dashed) line shows the 3 dB bandwidth obtained from Eq. (2) (assuming $H(\omega) = 1$) for a spontaneous emission lifetime of $\tau_e = 1.77$ ns ($\tau_e = 11$ ps) corresponding to the material used throughout this paper (respectively, for possible Purcell enhanced materials; see text). The open circles indicate commercially available Si photodiodes from several commercial vendors [14]. For the photodiodes the detector length is taken as the square root of the active area. (b) Step response measured with a fast photodiode: the green (blue) dots show the optical response of the fluorescence (excitation) signal. The red line is a fit to an exponential decay with a time constant of $\tau_e = 1.77$ ns. (c) Frequency response of the material measured with a fast photodiode. The red line corresponds to a Lorentzian fit with a 3 dB bandwidth of $f_{-3\,\mathrm{dB}} = 1/(2\pi\tau_e) = 91$ MHz. The slow, first-order gain roll-off allows for the use of frequency-division multiplexing techniques over a spectrum much larger than $f_{-3\,\mathrm{dB}}$.

B. Communication Link Demonstration

We demonstrate the communication capabilities of the LD shown in Fig. 1(b). We illuminate the detector with a large elliptical Gaussian beam with a horizontal (vertical) $1/e^2$ radius of 8.6 cm (1.3 cm), respectively, and a peak intensity of 0.9 mW/cm^2. Note that this value is below the eye-safety limit [15]. The intrinsic bandwidth limitation imposed by the response of the material can result in intersymbol interference and other deleterious effects that can limit reliable communications. To overcome this, digital modulation techniques designed for band-limited channels are employed. The slow decrease of the gain of the material for higher frequencies [see Fig. 2(c)] allows the use of modulation frequencies well above the 3 dB bandwidth, $f_{-3\,\mathrm{dB}}$. To maximally use the available spectrum, we employ orthogonal frequency division multiplexing (OFDM) [16], a modulation technique that consists of the superposition of equally spaced frequency subchannels of independently modulated data. The modulation scheme in each subchannel is selected to maximize the data rate by choosing the highest order modulation that can be supported by the signal-to-noise ratio (SNR) in that channel, a selection process known as bit loading. Given that the symbol duration in each subchannel is equal and that the modulation

order changes in discrete steps, the SNR in each subchannel exceeds what is required for reliable communication; to exactly match the modulation for each subchannel to the SNR, the transmit power in each subchannel can be adjusted in a technique known as power loading. Here, we split the spectrum into 102 subchannels spaced by 3.9 MHz, spanning a total bandwidth of 400 MHz. Figure 3(a) shows the SNR for the subchannels. Each subchannel is modulated with a different scheme, ranging from QAM-256 [see sample constellation in Fig. 3(e)] for channels with high SNR, to BPSK [Fig. 3(f)] for channels with low SNR. In addition to bit loading of the subchannels, we perform power loading on each subchannel to maximally optimize the throughput and bit error rates [see Fig. 3(b)]. By using this method we achieve a throughput of 2.109 Gbps with a bit error rate (BER) of 0.96×10^{-3}; the BER performance meets the unencoded BER necessary for a standard forward error correction (FEC) code to correct these errors [17,18]. By slightly reducing the size of the beam to $1/e^2$ horizontal (respectively, vertical) radius of 2.5 cm (respectively, 0.9 cm) to better collect the source power, we achieve a throughput of 2.357 Gbps and a BER of 0.82×10^{-3}. This slight increase of throughput indicates only a modest sensitivity of the throughput to the beam size. We also verify that the amplitude of the electrical signal is insensitive to the incident angle of the source beam over a range of ±25° and the horizontal position of the illumination region over a range ∼10 cm, set by the detector length. The increased field of view of the LD also increases the detected background light; however, for our conditions, taken under normal indoor lighting, this was a negligible contribution to the noise floor (see Supplement 1).

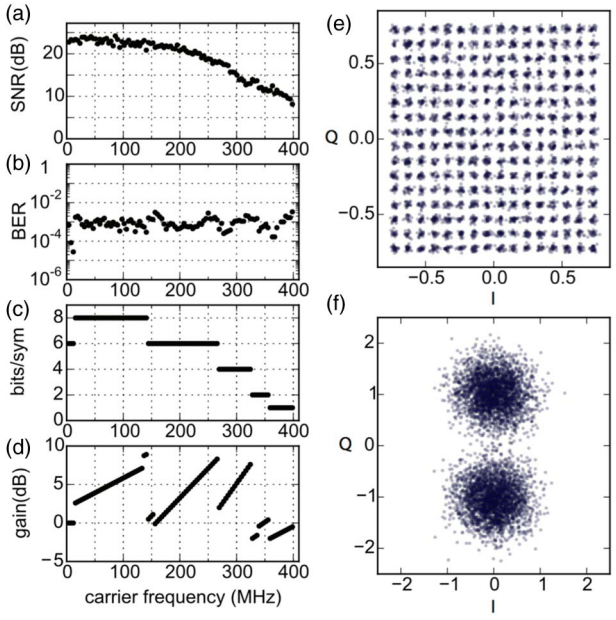

Fig. 3. OFDM implementation resulting in a total throughput of 2.109 Gbps and an unencoded BER of 0.96×10^{-3}. Left column: each subchannel has a width of 3.9 MHz; (a)–(d) show the SNR, BER, bit loading, and power loading for each subchannel, respectively. Right column: (e) QAM-256 and (f) BPSK (bottom) constellations of the 12th (50.78 MHz) and 98th (386.72 MHz) subchannels, respectively. The optimization procedure is performed by varying the bit and power loading to achieve a BER of $\sim 10^{-3}$ for each subchannel. The discontinuities in the gain near 150 MHz and 340 MHz for constant bit loading result from adjustments to flatten the BER.

C. Omnidirectional Detector

We further demonstrate the potential of LDs for communication applications requiring omnidirectional sensitivity, such as with diffuse light sources or highly mobile applications. The flexible nature of the plastic optical fibers makes it very straightforward to fabricate other detector shapes optimized for different applications. Here, we assemble a bundle of wavelength shifting fibers in a spherical shape, resulting in a nearly identical cross section from any angle, as illustrated by Fig. 4(a). We measure the optical antenna gain as a function of the polar (θ) and azimuthal (ϕ) angle. For comparison, we also show the angular dependence of the gain of the bare photodiode and of a typical lens ($f = 50$ mm) with the same aperture as the spherical LD detector ($D = 50$ mm). Comparing the bare photodiode and the LD cases, the losses from the absorption and re-emission process are nearly all compensated for by the increase in active area with the addition of omnidirectional sensitivity, even if the photodiode partly blocks the excitation light. The lens has a 18 dB higher gain than the LD, but the field of view (given by the solid angle where the gain is larger

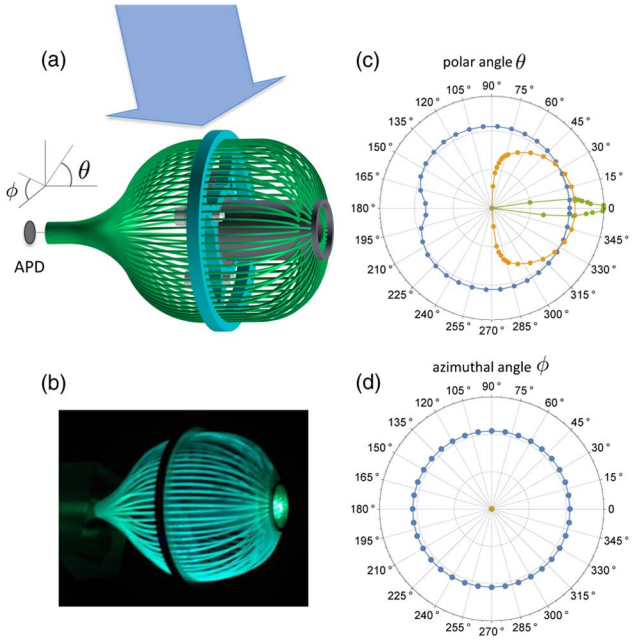

Fig. 4. (a) Experimental results for a LD with omnidirectional sensitivity: a bundle of fibers is arranged in a spherical geometry ($\phi = 50$ mm) to have an identical cross section from all directions. The light coming out of the fiber bundle is detected by a photodiode with a matching diameter of $\phi = 5$ mm. (b) Photograph of the detector under illumination. (c) and (d) Polar plots of the measured optical antenna gain for the polar and azimuthal angles, respectively. The blue data show the omnidirectional receiver, while the yellow show the response of the bare diode and the green show a lens with the same diameter as the omnidirectional receiver. The circular gridlines are in steps of 20 dB. The standard deviation in the antenna gain averaged over all angles is 1.9 and 0.2 dB for the polar and azimuthal angles, respectively. The depression in the antenna gain near $\theta = 180°$ is due to obstruction by the photodiode mount, which has a diameter of 25 mm. For $\theta = 0$, the antenna gain of the LD is 2.5 dB less than the bare diode, due to the losses arising from the LD, and 18 dB less than the $D = 50$ mm lens. For the azimuthal angle, the polar angle is set to $\theta = 90°$ and the bare photodiode and lens measurements have a gain equal to zero. The fields of view are $1.3 \times 10^{-3}\pi$, 0.33π, and 3.9π for the lens, bare photodiode, and LD, respectively.

than half of the maximum value) is 3.4×10^{-4} of that of the LD (see Fig. 4). The theoretical maximum optical antenna gain in a refractive optical system is achieved by using an optical system with a numerical aperture of NA = 1 on the photodiode side, set by the conservation of étendue. A compound parabolic concentrator (CPC), is an example of such an optical system, where the acceptance angle θ and input aperture A_{CPC} are related to the photodiode active area as $A_{\mathrm{CPC}}/A_{\mathrm{PD}} = n_{\mathrm{CPC}}^2/\sin^2\theta$, where n_{CPC} is the refractive index of the CPC. For our case, where $A_{\mathrm{CPC}} = \pi \times 25^2$ mm^2 and a typical value of $n_{\mathrm{CPC}} = 1.5$, this would correspond to a field of view of 2.4×10^{-2} and a maximum gain similar to that of the lens. Therefore, the luminescent material strongly improves the field of view over optical systems that conserve étendue.

3. DISCUSSION

Several improvements can be made to build upon these results and reach even higher data rates. Most importantly, the LDs presented here are fabricated using commercially available materials that have not been optimized for communication purposes. Photoluminescent materials that absorb in the (near)-infrared and have faster decay times would enable much higher data rates, as well as communication channels invisible to the human eye, and have yet to be developed. Materials that absorb above 1400 nm are of particular interest, since the eye-safe exposure limits are much higher [15], therefore allowing higher transmit powers.

In addition to material improvements, technical improvements can be made to increase the collection efficiency. The capture efficiency can be increased up to tens of percent for each propagation direction into the waveguide by tailoring the cladding with higher refractive index contrast, multiple layers, or Bragg reflectors [19]. The light emitted from the facet can be collected with higher efficiency using nonimaging optics, such as a CPC. For our geometry, a CPC would allow lossless light collection between the output of the fiber bundle and the photodiode, provided the CPC is bonded to the photodiode to avoid losses by total internal reflection at the output facet of the CPC due to an air gap.

Using a geometry similar to Fig. 1 and a CPC with a refractive index of n_{CPC}, the light collection gain becomes

$$G_{\mathrm{LD}} = \frac{L}{t}\frac{n_{\mathrm{CPC}}^2}{n_{\mathrm{co}}^2 - n_{\mathrm{cl}}^2}\eta_{\mathrm{cnv}}, \tag{3}$$

which can be as large as $\sim 10^3$ for a quantum efficiency approaching 1 and $\eta_c \sim 0.1$, since L can be many orders of magnitude larger than t. The thickness t is determined by the density of the dye molecules; therefore, it can be decreased by increasing the dye concentration. Higher dye concentrations will eventually lead to re-absorption of the re-emitted light, but this is typically small due to the large Stokes shift [see Fig. 1(c)], and, for typical detector sizes, the detector length is smaller than the characteristic absorption length (>3.5 m for our material [20]). Hence, the effective active aperture and the gain of the LD can be multiple orders of magnitude larger than the corresponding photodiode while maintaining omnidirectional sensitivity and large bandwidth.

A few more advantages of the LD are worth noting. First, long-range atmospheric communication channels experience scintillation effects. Atmospheric turbulence causes phase fluctuations of the optical wavefront, which results in severe fading effects, because the highly multimode beam cannot be easily focused onto a small photodiode. A large and fast LD is promising to suppress these effects. Additionally, the absorption and re-emission event destroys the coherence of the incident phase front and can therefore mitigate phase fluctuations, as well. In such communication systems, deep fades occur, typically 10 s of decibels. Depending on the conditions, a reduction in variance in the received signal power is of great importance despite the reduced detection efficiency. Reduced fluctuations equate to a smaller dynamic range in the detected signal power, which can simplify receiver operations.

Second, using fluorophores with narrow absorption and emission spectra would enable wavelength division multiplexing. This is of particular interest for visible light communication, which has been demonstrated using red, green, and blue multiplexing and targets indoor applications. Third, while we have demonstrated LDs using only optical fiber geometries, the same concept can also be applied to materials without guided modes. Recently, plasmonic nano arrays have been used to create highly directional emission from a layer of fluorescent dyes [21]. The emission of these materials has a relatively small étendue, which implies that it can be focused onto a small detector. This geometry could strongly increase the efficiency compared to the waveguide geometry. In addition, by leveraging the Purcell effect in plasmonic materials, the radiative lifetime of the photoluminescent centers can be decreased by almost 3 orders of magnitude, as fast as $\tau_e = 11$ ps, while preserving a high quantum efficiency [22]. These materials would allow communication with a 3 dB bandwidth in excess of 10 GHz, promising data rates of the order of 100 Gbps using spatial or wavelength division multiplexing or higher order modulation schemes such as presented in this paper.

In conclusion, we have shown that LDs offer important opportunities for communication applications. We have demonstrated more than 3 orders of magnitude increase of the active area of a detector, shown omnidirectional sensitivity, and demonstrated that multi-Gbps data rates can be achieved with standard modulation schemes. The addition of the luminescent material induces a band-limiting effect and a reduction in detection efficiency. We have presented various promising paths forward for both increased bandwidth and efficiency by more than 1 order of magnitude. Future research will be focused on developing tailored materials optimized for communication applications.

Funding. Facebook, Inc.

Acknowledgment. We thank K. Birnbaum, J. Goodman, H. Hemmati, Y. Maguire, H. Tiecke, and J. T. M. Walraven for insightful discussions and careful reading of the paper; J. W. Gin and D. H. Nguyen for developing the TIA; and E. Booen for mechanical design.

See Supplement 1 for supporting content.

REFERENCES AND NOTES

1. O. Bouchet, H. Sizun, C. Boisrobert, F. de Fornel, and P. N. Favennec, *Free-Space Optics: Propagation and Communication* (Wiley, 2006).
2. N. Zhao, X. Li, G. Li, and J. M. Kahn, "Capacity limits of spatially multiplexed free-space communication," Nat. Photonics **9**, 822–826 (2015).
3. J. Wang, J.-Y. Yang, I. M. Fazal, N. Ahmed, Y. Yan, H. Huang, Y. Ren, Y. Yue, S. Dolinar, M. Tur, and A. E. Willner, "Terabit free-space data transmission employing orbital angular momentum multiplexing," Nat. Photonics **6**, 488–496 (2012).
4. H. Hemmati, *Deep Space Optical Communications* (Wiley, 2006).

5. H. Hemmati, *Near-Earth Laser Communications* (CRC Press, Taylor & Francis, 2009).
6. http://fbnewsroomus.files.wordpress.com/2014/03/connecting-the-world-from-the-sky1.pdf.
7. D. O. Caplan, "Laser communication transmitter and receiver design," J. Opt. Fiber. Commun. Rep. **4**, 225–362 (2007).
8. G. Smestad, H. Ries, R. Winston, and E. Yablonovitch, "The thermodynamic limits of light concentrators," Sol. Energy Mater. **21**, 99–111 (1990).
9. W. G. J. H. M. van Sark, L. W. J. Barnham, L. H. Slooff, A. J. Chatten, A. Büchtemann, A. Meyer, S. J. McCormack, R. Koole, D. J. Farrell, R. Bose, E. E. Bende, A. R. Burgers, T. Budel, J. Quilitz, M. Kennedy, T. Meyer, C. De Mello Donegá, A. Meijerink, and D. Vanmaekelbergh, "Luminescent solar concentrators—a review of recent results," Opt. Express **16**, 21773–21792 (2008).
10. Y. N. Kharzheev, "Scintillation counters in modern high energy physics experiments," Phys. Part. Nucl. **46**, 678–728 (2015).
11. Z. Ghassemlooy, *Optical Wireless Communications* (CRC Press, 2013).
12. S. Dimitrov and H. Haas, *Principles of LED Light Communications* (Cambridge University, 2015).
13. $\mathrm{NEP_{APD}} = 6.5\ \mathrm{pW}/\sqrt{\mathrm{Hz}}$, corresponding to $\mathrm{NEP_{LD}} = 2.2\ \mathrm{nW}/\sqrt{\mathrm{Hz}}$, note that the LD has an active area more than three orders of magnitude larger than that of the APD, therefore the NEP of both detectors cannot be directly compared.
14. The data points are taken from the Hamamatsu, EO Tech, and Thorlabs catalogs.
15. "Safety of laser products—Part 1: Equipment classification and requirements," IEC 60825-1 (2014).
16. J. Armstrong, "OFDM for optical communications," J. Lightwave Technol. **27**, 189–204 (2009).
17. B. P. Smith, A. Farhood, A. Hunt, F. R. Kschischang, and J. Lodge, "Staircase codes: FEC for 100 Gb/s OTN," J. Lightwave Technol. **30**, 110–117 (2012).
18. G. Tzimpragos, C. Kachris, I. B. Djordjevic, M. Cvijetic, D. Soudris, and I. Tomkos, "A survey on FEC codes for 100 G and beyond optical networks," in *Communications Surveys and Tutorials* (IEEE, 2014).
19. The capture efficiency for a round fiber is given by $\eta_c = (1/2)(1 - (n_{\mathrm{cl}}/n_{\mathrm{co}}))$, which amounts to 17% in each direction for a vacuum clad $(n_{\mathrm{cl}} = 1)$ polystyrene $(n_{\mathrm{co}} = 1.6)$ fiber.
20. Saint Gobain Crystals, Scintillating Optical Fibers Brochure (2015).
21. G. Lozano, D. J. Louwers, S. R. K. Rodríguez, S. Murai, O. T. A. Jansen, M. A. Verschuuren, and J. Gómez Rivas, "Plasmonics for solid-state lighting: enhanced excitation and directional emission of highly efficient light sources," Light **2**, e66 (2013).
22. T. B. Hoang, G. M. Akselrod, C. Argyropoulos, J. Huang, D. R. Smith, and M. H. Mikkelsen, "Ultrafast spontaneous emission source using plasmonic nanoantennas," Nat. Commun. **6**, 7788 (2015).